



Long-term Multiband Near-infrared Variability of the Blazar OJ 287 during 2007–2021

Alok C. Gupta^{1,2} , Pankaj Kushwaha^{3,1,11} , L. Carrasco⁴, Haiguang Xu^{2,5} , Paul J. Wiita⁶ , G. Escobedo⁴, A. Porras⁴, E. Recillas⁴, Y. D. Mayya⁴ , V. Chavushyan⁴ , Beatriz Villarroel^{7,8}, and Zhongli Zhang^{9,10}

¹ Aryabhata Research Institute of Observational Sciences (ARIES), Manora Peak, Nainital—263001, India; acgupta30@gmail.com, pankaj.tifr@gmail.com

² Shanghai Frontiers Science Center of Gravitational Wave Detection, 800 Dongchuan Road, Minhang, Shanghai 200240, People's Republic of China; hgxu@sju.edu.cn

³ Department of Physical Sciences, Indian Institute of Science Education and Research Mohali, Knowledge City, Sector 81, SAS Nagar, Punjab 140306, India

⁴ Instituto Nacional de Astrofísica, Óptica y Electrónica, Luis Enrique Erro 1, Tonantzintla, Puebla, C.P. 72840, Mexico

⁵ School of Physics and Astronomy, Shanghai Jiao Tong University, 800 Dongchuan Road, Minhang, Shanghai 200240, People's Republic of China

⁶ Department of Physics, The College of New Jersey, 2000 Pennington Road, Ewing, NJ 08628-0718, USA

⁷ Nordita, KTH Royal Institute of Technology and Stockholm University, Roslagstullsbacken 23, SE-106 91 Stockholm, Sweden

⁸ Instituto de Astrofísica de Canarias, Avda Via Lactea S/N, La Laguna, E-38205, Tenerife, Spain

⁹ Shanghai Astronomical Observatory, Chinese Academy of Sciences, Shanghai 200030, People's Republic of China

¹⁰ Key Laboratory of Radio Astronomy, Chinese Academy of Sciences, 210033 Nanjing, Jiangsu, People's Republic of China

Received 2022 February 21; revised 2022 April 16; accepted 2022 May 1; published 2022 June 17

Abstract

We present the most extensive and well-sampled long-term multiband near-infrared (NIR) temporal and spectral variability study of OJ 287, considered to be the best candidate binary supermassive black hole blazar. These observations were made between 2007 December and 2021 November. The source underwent $\sim 2\text{--}2.5$ mag variations in the J , H , and K_s NIR bands. Over these long-term timescales there were no systematic trends in either flux or spectral evolution with time or with the source's flux states. However, on shorter timescales, there are significant variations in flux and spectra indicative of strong changes during different activity states. The NIR spectral energy distributions show diverse facets at each flux state, from the lowest to the highest. The spectra are, in general, consistent with a power-law spectral profile (within 10%) and many of them indicate minor changes (observationally insignificant) in the shift of the peak. The NIR spectra generally steepen during bright phases. We briefly discuss these behaviors in the context of blazar emission scenarios/mechanisms, OJ 287's well-known traditional behavior, and implications for models of the source central engine invoked for its long-term optical semiperiodic variations.

Unified Astronomy Thesaurus concepts: Galaxies (573); BL Lacertae objects (158)

Supporting material: animation

1. Introduction

Blazars, referring to the union of BL Lacertae objects (BL Lacs) and flat-spectrum radio quasars, are a subclass of radio-loud active galactic nuclei (AGNs) that host a large-scale relativistic jet of plasma pointing almost in our direction (Urry & Padovani 1995). The jet is launched very near to the core formed by a central supermassive black hole (SMBH) of mass in the range of $10^6\text{--}10^{10} M_\odot$ and the plasma around it (Woo & Urry 2002). Blazars are known for perennial dynamic variability, characterized by rapid and strong flux variations in their emission that spans the entire electromagnetic spectrum from radio up to γ -rays; that emission exhibits a broad bimodal spectral energy distribution (SED) (Fossati et al. 1998). The lower-energy hump is attributed to synchrotron emission from relativistic leptons and the higher-energy hump to inverse Compton or hadronic processes (e.g., Marscher 1983; Mücke et al. 2003; Romero et al. 2017, and references therein).

Variability across the complete electromagnetic (EM) spectrum has been a key component in the definition of blazars and is not only limited to flux but encompasses all the directly

accessible observables. Blazar EM emission is predominantly nonthermal. In the absence of adequate spatial resolution, temporal flux variability is used to infer spatial scales of the emission region. Studies of the fluxes of blazars have found them to be variable on almost all accessible timescales from the order of a few minutes to decades and more. In general, variability has been categorized into three subclasses: intraday variability (IDV) focusing on variability over a day or less (Miller et al. 1989; Wagner & Witzel 1995), short-term variability focusing on variability over days to several weeks, and long-term variability (LTV) focusing on timescales of months to years (Gupta et al. 2004).

The BL Lac blazar OJ 287 ($\alpha_{2000.0} = 08^{\text{h}}54^{\text{m}}48^{\text{s}}.87$, $\delta_{2000.0} = +20^{\circ}06'30''.64$) is at redshift $z = 0.306$ (Sitko & Junkkarinen 1985). Optical observational data on this source actually date back to 1888 and using this century-long light curve (LC), Sillanpää et al. (1988) noticed for the first time that the source appeared to show double-peaked outburst features which repeated with a period of ~ 12 yr. To explain this nominal quasiperiodic oscillation (QPO) feature in the long-term optical LC, Sillanpää et al. (1988) proposed a binary SMBH system for the blazar and predicted that the next double-peaked outburst would occur in 1994–1995. An extensive global observing campaign called OJ-94 was organized and the predicted double-peaked outbursts were really observed, with the second peak being detected ~ 1.2 yr after the first one (Sillanpää et al. 1996a, 1996b). The OJ-94

¹¹ DST-INSPIRE Faculty Fellow.

project supported the basic model prediction but also revealed rather sharp rises of the predicted flares, which led to a major modification of the model, with the outbursts now attributed to the impact of the secondary SMBH on the accretion disk of the primary (Lehto & Valtonen 1996). Apart from this apparently well-established QPO, OJ 287 is the blazar with the highest number of claims of QPOs on a wide range of timescales, from a few tens of minutes to decades and more across many EM bands (e.g., Visvanathan & Elliot 1973; Carrasco et al. 1985; Valtaoja et al. 1985; Sillanpää et al. 1988; Bhatta et al. 2016; Britzen et al. 2018; Kushwaha et al. 2020, and references therein).

In the observing campaign of OJ 287 during 2005–2007, the double-peaked outbursts were detected respectively at the end of 2005 and end of 2007, i.e., separated by ~ 2 yr (Valtonen et al. 2009). For the most recent predicted double-peaked outbursts, the first and second outbursts were observed in 2015 December and 2019 July, respectively, i.e., separated by ~ 3.5 yr (Valtonen et al. 2016; Gupta et al. 2017; Laine et al. 2020). The continued theoretical and observational efforts following this have led to better constraints on the timings of these outbursts and thus the model as well. The latest iteration of the model incorporating improved treatment of dynamics with more physical aspects related to strong gravity and its consequences on the timing of the QPOs is presented in Dey et al. (2018). Alternative interpretations of these recurrent outbursts invoke simple jet precession scenarios (e.g., Britzen et al. 2018; Butuzova & Pushkarev 2020, and references therein). The jet precession models, however, are not favored by the spectral changes reported in the near-infrared (NIR) to γ -rays during and after the most recent outbursts of 2015 (Komossa et al. 2017, 2020; O’Brien 2017; Kushwaha et al. 2018a, 2018b; Pal et al. 2020) and 2019 (Komossa et al. 2020; Kushwaha et al. 2021; Singh et al. 2022). The timing of the most recent outbursts (2015 and 2019) considered within the binary disk-impact model indicates the significant effect of gravitational-wave (GW) energy loss. Detailed modeling suggests the rate of orbital shrinkage induced by GW emission is $\sim 10^{-3}$ and has a nonnegligible effect on the timing of this QPO (Dey et al. 2018). OJ 287 or other AGNs possessing close binary SMBHs are eventual candidates for direct detection of GW emission by the Pulsar Timing Array or an interferometer in space (e.g., Chen & Zhang 2018; Baker et al. 2019a, 2019b; Burke-Spolaor et al. 2019).

Early studies found OJ 287 to be the most dynamically variable BL Lac object, exhibiting correlated multiwavelength variability (e.g., Sitko & Junkkarinen 1985; Fan et al. 1998, and references therein). In NIR bands, OJ 287 has been studied occasionally (Holmes et al. 1984a, 1984b; Gear et al. 1986; Takalo et al. 1992), but these studies have normally been limited to the duration of an ongoing enhanced activity period (Gear et al. 1986; Pursimo et al. 2000; Kushwaha et al. 2018a) and the very few done over a longer (\gtrsim years) duration generally have very sparse data sampling (Bonning et al. 2012; Sandrinelli et al. 2014). In the very first coordinated radio, NIR, and optical monitoring, a $\sim 25\%$ IDV variation at NIR was reported, slightly less than in the optical (Epstein et al. 1972). In another study at NIR with the United Kingdom Infra Red Telescope, strong brightness variations in J , H , and K bands, along with some unusual $J-H$ and $H-K$ color variations, were found (Wolstencroft et al. 1982). Motivated by this result, further monitoring in the J band with a temporal resolution of

5 s revealed a 1 mag brightness change in 50 s—the fastest and strongest variation in any BL Lac at that time. In a photopolarimetric study during an outburst state in 1983, strong variation in flux as well as polarization and an energy-dependent variation in polarization was seen (Holmes et al. 1984a, 1984b). Also, an excellent correlation between IR flux and spectral index, in the sense that as the source gets fainter the spectrum gets steeper and vice versa, was found (Gear et al. 1986). In 1993–1994, a continuous increase in NIR brightness was seen, with the maximum brightness a factor of 3 higher since the start of monitoring. Smaller flares with an amplitude of up to 1 mag were seen on timescales of a few days (Kidger et al. 1995; Pursimo et al. 2000). Though early studies are quite sparsely sampled and limited at most to a few days, the compiled data show strong flux as well as spectral variations with a brightness change of $\gtrsim 3.5$ mag between the extremes at NIR bands, i.e., by a factor of $\gtrsim 25$ in flux (Litchfield et al. 1994; Fan et al. 1998, and references therein).

Later studies employing simultaneous NIR–optical data, much better sampled than previous ones, and spanning over timescales of a few years report magnitude variability of around 2, or flux variations of $\gtrsim 6$ times, between the extremes, with the NIR changes slightly less than those in the optical (Bonning et al. 2012; Sandrinelli et al. 2014). Significant spectral changes at NIR energies as well as a hysteresis between NIR and optical color variation have also been reported (Bonning et al. 2012). In terms of strong all-around changes in observational behavior, the period around the latest double-peaked outburst has been remarkable (Gupta et al. 2017, 2019; Kushwaha et al. 2018a, 2021; Singh et al. 2022). However, the data used in these studies are mostly biased toward high-activity states.

The study of blazar variability on diverse timescales across the complete EM spectrum is a prominent area of research in modern astronomy and astrophysics. The NIR variability of blazars is comparatively less explored than many other bands due to the paucity of NIR ground-based telescopes. For building a NIR telescope, one requires an observing site with low humidity, which most ground-based observatories do not have. We have access to a 2.12 m NIR telescope at an excellent observing site in Mexico. We started a pilot project to study blazars’ temporal and spectral variabilities on diverse timescales in NIR bands in isolation and/or with associated multiwavelength observations. Under the project, here we present the first densely sampled multiband long-term NIR temporal and spectral variability study of the blazar OJ 287 from 2007 December 18–2021 November 13. A multiwavelength study reporting the spectral and temporal behavior will be presented in follow-up work (P. Kushwaha et al. 2022, in preparation) that will deal with the vastly different sampling and data integration times in different portions of the EM spectrum.

In Section 2, we provide brief information about the observing facility, data acquisition, and reduction. In Section 3, we present our results, and in Section 4 we give a discussion followed by a summary.

2. Observations and Data Reduction

The data of OJ 287 used in this paper are part of the INAOE¹² NIR monitoring program of blazars that started in

¹² Instituto Nacional de Astrofísica, Óptica y Electrónica, Mexico.

2005 (L. Carrasco et al. 2022, in preparation) and have been graciously provided by the members of the program.

These new J -, H -, and Ks -band NIR photometric observations were obtained with the 2.12 m telescope of the Guillermo Haro Astrophysical Observatory (OAGH) located in Cananea, Sonora, Mexico. The telescope is equipped with an NIR camera named CANICA (the Cananea Near-Infrared Camera) which operates at multiple bands, including the J (1.24 μm), H (1.63 μm) and Ks (2.12 μm) broad bands.

The camera is a 1024 pixel \times 1024 pixel format HgCdTe Hawaii II array of 18.5 $\mu\text{m} \times$ 18.5 μm pixel size, covering a field of view of $5' \times 5'$ for a plate scale $0''.32 \text{ pixel}^{-1}$ in the sky (Carrasco et al. 2017). The frames were dark subtracted, flat fielded, and obtained at seven dithered positions in the sky in a sequential manner for the filter's H , J , and Ks bands. Those frames were then median sky subtracted and finally, after shifting and registering, were coadded. Relative photometry is obtained for every coadded frame to the photometric values for point sources listed in the Two Micron All Sky Survey (2MASS) in the field of view of the camera.

For OJ 287 the dithered images had typical exposure times of 30 s, yielding total integration times of 210 s for each filter. The number of comparison sources was typically 10. In general, probable errors are 0.04, 0.03, and 0.04 mag in J , H , and Ks bands, respectively. The present data sample comprises ~ 520 individual observations. These data, after correcting for reddening following Cardelli et al. (1989), are reported in Table 1.

3. Results

In Figure 1 we present the J -, H -, and Ks -band NIR photometric LCs generated from our new observations taken during 2007 December–2021 November. This is the most extensive and well-sampled long-term NIR photometric study of the blazar OJ 287. On visual inspection the J -, H -, and Ks -band LCs all clearly show large-amplitude flux variations. Several substantial flaring events in the photometric observations in all three bands are seen. In the following subsections, we discuss the NIR temporal and spectral variability properties of the blazar OJ 287 on LTV timescales.

3.1. LC Analysis Techniques

To calculate the amplitude of LTV variability and interband cross correlations in the NIR J , H , and Ks bands, the methods we used are briefly described below.

3.1.1. Amplitude of Variability

The percentage of the amplitude of the variability in magnitude (and color) on LTV timescales is described by the parameter, A , which can be defined using the following equation introduced by Heidt & Wagner (1996):

$$A = 100 \times \sqrt{(A_{\max} - A_{\min})^2 - 2\sigma^2} (\%). \quad (1)$$

Here A_{\max} and A_{\min} are the maximum and minimum values, respectively, in the calibrated magnitude or color of the LC of the blazar, and σ is the mean measurement error.

3.1.2. Discrete Cross Correlation Function

We carried out the cross correlation analysis between the NIR bands using the z -transformed discrete cross correlation (zDCF; Alexander 1997, 2013) method. It is broadly similar to

the traditional DCF except that the correlation coefficient errors are estimated using the z -transform, given by

$$z = \frac{1}{2} \ln \left(\frac{1+r}{1-r} \right), \quad \zeta = \frac{1}{2} \ln \left(\frac{1+\rho}{1-\rho} \right), \quad r = \tanh(z), \quad (2)$$

where r and ρ represent the bin correlation coefficient and the unknown population correlation coefficient, respectively. The correlation coefficients are estimated by constructing all possible time-lag data pairs (x_i, y_i) between the two LCs as

$$r = \frac{\sum_i^n (x_i - \bar{x})(y_i - \bar{y})}{\sigma_x \sigma_y}, \quad s_x^2 = \frac{1}{n-1} \sum_i^n (x_i - \bar{x})^2. \quad (3)$$

In order to obtain the mean and variance of z , $\rho = r$ is assumed (Alexander 2013). The reason for making the z -transformation is that the correlation coefficients are not normally distributed in the real space. This method is applicable to both uniformly and sparse, nonuniformly, sampled time-series data. It employs Fisher's z -transform and equal population binning to handle the bias arising due to sampling and skewness and fares better compared to the traditional approaches (Alexander 1997, 2013). The errors were estimated using the Monte Carlo method by simulating 1000 pairs of LCs from the observed LCs by adding a Gaussian noise extracted from the measured error bars. The resulting cross correlation results are shown in Figure 2. The peaks at zero lag signify that the multiband NIR variations are simultaneous.

3.2. Long-term Variability

Our typical observational cadence of once a month, with a daily follow-up around the higher activity phases, allows us to explore long-term variations of OJ 287 in multiband NIR flux, color, spectral index, and SEDs. We also discuss the detection of a large number of flaring events during the whole observing duration.

3.2.1. Flux Variability

Large-amplitude significant flux variability from OJ 287 on LTV timescales is clearly visible from the three panels of Figure 1, where the J -, H -, and Ks -band LCs are presented from the bottom to top panels, respectively. We have calculated the variability amplitudes in the J , H , and Ks NIR photometric bands, and the results are reported in Table 2. We found the faintest levels of the blazar in the J , H , and Ks bands were 13.846 mag at JD 2,456,314.995185, 12.957 mag at JD 2,456,304.915382, and 12.645 mag at JD 2,455,363.648433, respectively. Similarly the observed brightest levels are 11.706 mag at JD 2,457,689.016863, 10.942 mag at JD 2,457,365.021296, and 10.053 mag at JD 2,457,365.027350, in the J , H , and Ks bands, respectively. In terms of fluxes, the amplitudes of variation given in Table 2 correspond to changes by a factor of roughly 7.2, 6.4, and 10.9 in the J , H , and Ks bands respectively. In the nearly 14 yr long NIR observational duration, the large-amplitude variations in the blazar LCs indicate that we have observed the source in low, intermediate, high, and possibly even outburst, flux states. Historically, the brightest reported NIR magnitudes of OJ 287 were $J=10.73$ mag, $H=9.94$ mag, and $K=8.81$ mag, with the faintest being $J=14.60$ mag, $H=13.73$ mag, and $K=12.75$ mag (Fan et al. 1998). If we compare them with our data presented here, it can be

Table 1
 Reddening-corrected NIR Data of OJ 287 between 2007 and 2021 (Reference Section 2)

| JD (2,450,000+) | J (mag \pm error) | JD (2,450,000+) | H (mag \pm error) | JD (2,450,000+) | K_s (mag \pm error) |
|--------------------|--------------------------|--------------------|--------------------------|--------------------|----------------------------|
| 4452.797360 | 12.105 \pm 0.03 | 4452.801526 | 11.276 \pm 0.03 | 4452.805692 | 10.942 \pm 0.03 |
| 4475.951106 | 11.798 \pm 0.04 | 4475.962679 | 11.045 \pm 0.03 | 4475.970317 | 10.301 \pm 0.03 |
| 4507.847707 | 12.179 \pm 0.03 | 4507.853436 | 11.307 \pm 0.02 | 4507.858968 | 10.636 \pm 0.04 |
| 4551.719372 | 12.704 \pm 0.03 | 4551.727011 | 11.844 \pm 0.05 | 4551.733261 | 11.005 \pm 0.02 |
| 4564.797741 | 13.021 \pm 0.04 | 4564.789940 | 12.150 \pm 0.03 | 4564.805738 | 11.270 \pm 0.02 |
| 4589.668243 | 12.850 \pm 0.05 | 4589.663381 | 12.040 \pm 0.05 | 4589.673104 | 11.166 \pm 0.01 |
| 4804.998881 | 12.627 \pm 0.05 | 4805.005826 | 11.658 \pm 0.06 | 4805.013466 | 10.842 \pm 0.03 |
| 4856.995965 | 12.542 \pm 0.03 | 4856.989390 | 11.638 \pm 0.06 | 4856.999784 | 10.689 \pm 0.03 |
| 4860.880016 | 12.718 \pm 0.02 | 4860.893905 | 11.750 \pm 0.03 | 4860.902932 | 10.866 \pm 0.03 |
| 4893.821950 | 12.240 \pm 0.03 | 4893.817714 | 11.272 \pm 0.05 | 4893.826394 | 10.421 \pm 0.03 |
| 4909.779554 | 13.002 \pm 0.03 | 4909.773652 | 12.179 \pm 0.04 | 4909.785109 | 11.184 \pm 0.06 |
| 4912.821687 | 12.917 \pm 0.05 | 4912.814049 | 11.997 \pm 0.05 | 4912.827937 | 11.025 \pm 0.05 |
| 4954.708825 | 13.388 \pm 0.05 | 4954.691466 | 12.497 \pm 0.05 | ... | ... |
| 4976.654647 | 13.474 \pm 0.01 | 4976.647703 | 12.494 \pm 0.06 | 4976.658119 | 11.616 \pm 0.03 |
| 5177.965478 | 12.137 \pm 0.03 | 5177.956449 | 11.227 \pm 0.05 | 5177.970339 | 10.396 \pm 0.04 |
| 5183.984137 | 12.232 \pm 0.03 | 5183.978685 | 11.325 \pm 0.06 | 5183.987737 | 10.607 \pm 0.04 |
| 5185.004181 | 12.142 \pm 0.03 | 5184.999551 | 11.370 \pm 0.06 | 5185.006264 | 10.619 \pm 0.05 |
| 5185.894403 | 12.189 \pm 0.03 | 5185.890352 | 11.291 \pm 0.02 | 5185.897991 | 10.522 \pm 0.05 |
| 5207.878302 | 12.091 \pm 0.09 | 5207.874830 | 11.233 \pm 0.07 | 5207.883858 | 10.471 \pm 0.08 |
| 5241.899977 | 12.293 \pm 0.06 | 5241.895533 | 11.421 \pm 0.04 | 5241.903450 | 10.707 \pm 0.02 |
| 5244.892790 | 12.226 \pm 0.02 | 5244.888160 | 11.476 \pm 0.06 | 5244.896158 | 10.897 \pm 0.07 |
| ... | ... | 5259.893016 | 11.702 \pm 0.06 | ... | ... |
| 5269.712567 | 12.709 \pm 0.03 | 5269.690346 | 11.905 \pm 0.06 | 5269.745203 | 11.298 \pm 0.09 |
| 5273.830616 | 12.741 \pm 0.05 | 5273.826866 | 11.940 \pm 0.03 | 5273.834366 | 11.303 \pm 0.09 |
| 5305.703974 | 13.234 \pm 0.02 | 5305.694947 | 12.247 \pm 0.04 | 5305.716472 | 11.616 \pm 0.11 |
| 5312.764392 | 13.432 \pm 0.04 | 5312.757448 | 12.604 \pm 0.03 | 5312.769947 | 11.937 \pm 0.12 |
| 5320.667784 | 13.175 \pm 0.01 | 5320.662924 | 12.367 \pm 0.05 | 5320.673339 | 11.603 \pm 0.02 |
| 5331.641018 | 13.486 \pm 0.06 | 5331.635463 | 12.638 \pm 0.03 | 5331.637546 | 11.829 \pm 0.07 |
| 5333.665130 | 13.788 \pm 0.04 | 5333.659876 | 12.907 \pm 0.06 | 5333.668047 | 12.193 \pm 0.02 |
| 5363.643642 | 13.324 \pm 0.01 | 5363.639892 | 12.533 \pm 0.04 | 5363.648433 | 12.636 \pm 0.19 |
| ... | ... | 5480.012163 | 12.576 \pm 0.01 | ... | ... |
| 5515.981656 | 12.885 \pm 0.04 | 5515.977489 | 11.991 \pm 0.01 | 5515.985615 | 11.213 \pm 0.09 |
| 5559.937581 | 13.059 \pm 0.03 | 5559.935405 | 12.513 \pm 0.01 | 5559.939711 | 11.514 \pm 0.03 |
| 5573.913484 | 12.838 \pm 0.03 | 5573.910127 | 12.006 \pm 0.07 | 5573.915822 | 11.232 \pm 0.04 |
| 5574.954757 | 12.574 \pm 0.04 | 5574.952245 | 11.824 \pm 0.07 | 5574.959965 | 11.167 \pm 0.05 |
| 5576.854051 | 12.767 \pm 0.06 | 5576.850683 | 11.957 \pm 0.04 | 5576.857130 | 11.094 \pm 0.07 |
| 5599.914132 | 12.733 \pm 0.07 | 5599.911829 | 11.916 \pm 0.05 | 5599.916493 | 11.016 \pm 0.04 |
| 5601.898171 | 12.795 \pm 0.04 | 5601.895613 | 11.894 \pm 0.04 | 5601.900463 | 11.044 \pm 0.06 |
| 5634.809086 | 13.180 \pm 0.02 | 5634.805822 | 12.351 \pm 0.04 | 5634.811655 | 11.681 \pm 0.04 |
| 5635.789826 | 13.128 \pm 0.03 | 5635.786736 | 12.317 \pm 0.03 | 5635.794549 | 11.587 \pm 0.04 |
| 5666.731273 | 13.126 \pm 0.02 | 5666.728565 | 12.304 \pm 0.06 | 5666.733773 | 11.391 \pm 0.07 |
| 5674.673090 | 13.183 \pm 0.04 | 5674.670093 | 12.538 \pm 0.04 | 5674.676609 | 11.757 \pm 0.02 |
| 5689.726944 | 13.106 \pm 0.03 | 5689.723935 | 12.260 \pm 0.02 | 5689.729919 | 11.494 \pm 0.08 |
| 5692.733819 | 13.202 \pm 0.05 | 5692.731273 | 12.396 \pm 0.04 | 5692.736343 | 11.812 \pm 0.07 |
| 5693.654502 | 13.146 \pm 0.05 | 5693.651944 | 12.341 \pm 0.07 | 5693.657384 | 11.641 \pm 0.07 |
| 5695.658877 | 13.072 \pm 0.09 | 5695.656389 | 12.260 \pm 0.04 | 5695.661424 | 11.493 \pm 0.11 |
| 5696.667708 | 13.057 \pm 0.07 | 5696.664583 | 12.257 \pm 0.04 | 5696.670671 | 11.470 \pm 0.07 |
| 5703.663021 | 13.191 \pm 0.03 | 5703.660729 | 12.401 \pm 0.07 | 5703.665046 | 11.659 \pm 0.07 |
| 6066.700995 | 12.238 \pm 0.07 | 6066.696111 | 11.446 \pm 0.07 | 6066.710139 | 10.714 \pm 0.04 |
| 6225.043171 | 13.086 \pm 0.09 | 6225.044977 | 12.306 \pm 0.09 | 6225.046632 | 11.903 \pm 0.09 |
| 6238.945556 | 12.869 \pm 0.07 | 6238.933958 | 12.365 \pm 0.05 | 6238.957002 | 11.406 \pm 0.08 |
| 6254.980648 | 12.891 \pm 0.04 | 6254.978009 | 12.011 \pm 0.06 | 6254.984063 | 11.410 \pm 0.09 |
| 6256.036019 | 13.143 \pm 0.04 | 6256.033646 | 12.349 \pm 0.06 | 6256.038472 | 11.825 \pm 0.04 |
| 6256.999641 | 13.483 \pm 0.03 | 6256.997130 | 12.532 \pm 0.05 | 6257.002269 | 12.039 \pm 0.06 |
| 6272.899988 | 13.369 \pm 0.03 | 6272.897095 | 12.523 \pm 0.05 | 6272.902824 | 11.890 \pm 0.09 |
| 6273.975336 | 13.594 \pm 0.05 | 6273.972315 | 12.673 \pm 0.04 | 6273.977882 | 11.898 \pm 0.07 |
| 6279.979630 | 13.629 \pm 0.05 | 6279.976354 | 12.707 \pm 0.05 | 6279.982813 | 12.020 \pm 0.12 |
| 6282.949213 | 13.587 \pm 0.03 | 6282.946111 | 12.766 \pm 0.07 | 6282.952465 | 12.294 \pm 0.08 |
| 6304.918600 | 13.824 \pm 0.04 | 6304.915382 | 12.944 \pm 0.03 | 6304.921910 | 12.256 \pm 0.04 |
| 6306.957569 | 13.714 \pm 0.04 | 6306.954745 | 12.832 \pm 0.05 | 6306.960278 | 12.204 \pm 0.05 |
| 6314.995185 | 13.825 \pm 0.02 | 6314.992731 | 12.912 \pm 0.06 | 6314.997662 | 12.514 \pm 0.05 |
| 6343.771204 | 12.733 \pm 0.04 | 6343.768623 | 11.925 \pm 0.04 | 6343.773796 | 11.346 \pm 0.11 |
| 6346.852350 | 12.596 \pm 0.05 | 6346.849653 | 11.745 \pm 0.06 | 6346.854815 | 11.020 \pm 0.08 |

Table 1
(Continued)

| JD (2,450,000+) | <i>J</i> (mag ± error) | JD (2,450,000+) | <i>H</i> (mag ± error) | JD (2,450,000+) | <i>K_s</i> (mag ± error) |
|--------------------|---------------------------|--------------------|---------------------------|--------------------|---------------------------------------|
| 6347.798472 | 12.890 ± 0.04 | 6347.793623 | 11.906 ± 0.05 | 6347.803472 | 11.422 ± 0.04 |
| 6353.789502 | 12.847 ± 0.05 | 6353.784005 | 11.932 ± 0.04 | 6353.794259 | 11.493 ± 0.03 |
| 6354.701076 | 12.856 ± 0.05 | 6354.695799 | 11.945 ± 0.04 | 6354.706400 | 11.459 ± 0.06 |
| 6386.725046 | 13.151 ± 0.03 | 6386.719734 | 12.335 ± 0.03 | 6386.730370 | 11.845 ± 0.06 |
| ... | ... | 6388.703796 | 12.358 ± 0.04 | ... | ... |
| 6401.692975 | 13.557 ± 0.05 | 6401.688738 | 12.637 ± 0.04 | 6401.696609 | 11.950 ± 0.07 |
| 6404.660370 | 13.191 ± 0.04 | 6404.656933 | 12.471 ± 0.02 | 6404.663924 | 11.783 ± 0.03 |
| 6416.702060 | 12.977 ± 0.06 | 6416.699630 | 12.043 ± 0.05 | 6416.704421 | 11.449 ± 0.09 |
| 6429.704456 | 12.935 ± 0.06 | 6429.701238 | 12.054 ± 0.06 | 6429.707951 | 11.541 ± 0.07 |
| 6595.031354 | 13.145 ± 0.04 | 6595.028958 | 12.663 ± 0.03 | 6595.033322 | 11.798 ± 0.04 |
| 6646.872130 | 13.428 ± 0.06 | 6646.869850 | 12.663 ± 0.05 | 6646.874329 | 11.866 ± 0.12 |
| 6660.967743 | 13.143 ± 0.06 | 6660.965532 | 12.245 ± 0.05 | 6660.969722 | 11.786 ± 0.06 |
| 6677.976331 | 13.450 ± 0.08 | 6677.974039 | 12.650 ± 0.03 | 6677.978530 | 11.810 ± 0.03 |
| 6697.906204 | 13.059 ± 0.02 | 6697.903854 | 12.272 ± 0.03 | 6697.908773 | 11.567 ± 0.05 |
| 6700.948924 | 12.630 ± 0.06 | 6700.946435 | 11.760 ± 0.05 | 6700.951042 | 10.962 ± 0.01 |
| 6707.850625 | 12.381 ± 0.04 | 6707.848333 | 11.535 ± 0.08 | 6707.852581 | 10.626 ± 0.05 |
| 6736.752569 | 12.946 ± 0.03 | 6736.750590 | 11.986 ± 0.08 | 6736.754664 | 11.107 ± 0.04 |
| 6750.772593 | 12.603 ± 0.07 | 6750.770799 | 11.733 ± 0.04 | 6750.774259 | 10.891 ± 0.06 |
| 6804.630799 | 13.670 ± 0.08 | 6804.628183 | 12.671 ± 0.07 | 6804.633009 | 11.807 ± 0.09 |
| 6978.973391 | 13.668 ± 0.07 | 6978.970498 | 12.749 ± 0.07 | 6978.976354 | 11.989 ± 0.06 |
| 6993.009502 | 13.587 ± 0.02 | 6993.006250 | 12.741 ± 0.04 | 6993.012986 | 11.798 ± 0.03 |
| 7007.018704 | 12.792 ± 0.04 | 7007.013889 | 12.029 ± 0.03 | 7007.023738 | 11.268 ± 0.06 |
| 7021.041123 | 12.849 ± 0.03 | 7021.039155 | 12.011 ± 0.05 | 7021.043090 | 11.289 ± 0.03 |
| 7032.954213 | 12.792 ± 0.02 | 7032.951887 | 12.004 ± 0.07 | 7032.956667 | 11.240 ± 0.02 |
| 7035.938623 | 12.839 ± 0.02 | 7035.936250 | 12.018 ± 0.02 | 7035.941146 | 11.323 ± 0.03 |
| 7079.808021 | 13.038 ± 0.03 | 7079.804618 | 12.230 ± 0.03 | 7079.812130 | 11.561 ± 0.05 |
| 7081.823090 | 13.098 ± 0.05 | 7081.820509 | 12.558 ± 0.05 | 7081.825799 | 11.637 ± 0.05 |
| 7095.869248 | 12.947 ± 0.03 | 7095.866748 | 12.181 ± 0.05 | 7095.871910 | 11.251 ± 0.04 |
| 7112.763403 | 12.991 ± 0.07 | 7112.761563 | 12.191 ± 0.04 | 7112.765347 | 11.502 ± 0.04 |
| 7121.772153 | 13.108 ± 0.09 | 7121.769063 | 12.159 ± 0.03 | 7121.774502 | 11.493 ± 0.08 |
| 7140.703819 | 12.891 ± 0.04 | 7140.700602 | 12.113 ± 0.03 | 7140.707350 | 11.405 ± 0.04 |
| 7154.708553 | 12.759 ± 0.03 | 7154.705637 | 11.945 ± 0.04 | 7154.711435 | 11.275 ± 0.04 |
| 7169.656632 | 13.288 ± 0.08 | 7169.653553 | 12.276 ± 0.06 | 7169.659340 | 11.794 ± 0.04 |
| 7332.964664 | 13.185 ± 0.03 | 7332.960799 | 12.316 ± 0.03 | 7332.968646 | 11.419 ± 0.03 |
| 7348.034618 | 13.017 ± 0.06 | 7348.032303 | 12.173 ± 0.03 | 7348.036887 | 11.444 ± 0.03 |
| 7362.930382 | 11.978 ± 0.03 | 7362.927535 | 11.115 ± 0.04 | 7362.933252 | 10.373 ± 0.03 |
| 7365.024826 | 11.768 ± 0.03 | 7365.021296 | 10.929 ± 0.04 | 7365.027350 | 10.044 ± 0.04 |
| 7365.971898 | 12.054 ± 0.03 | 7365.968808 | 11.188 ± 0.03 | 7365.974838 | 10.495 ± 0.03 |
| 7373.960440 | 12.347 ± 0.05 | 7373.955752 | 11.547 ± 0.03 | 7373.964803 | 10.696 ± 0.04 |
| 7375.011076 | 12.606 ± 0.03 | 7375.008565 | 11.659 ± 0.05 | 7375.013438 | 10.997 ± 0.05 |
| 7376.013507 | 12.450 ± 0.05 | 7376.006389 | 11.515 ± 0.04 | 7376.020926 | 10.822 ± 0.06 |
| 7378.038900 | 12.318 ± 0.04 | 7378.035880 | 11.424 ± 0.04 | 7378.041516 | 10.704 ± 0.06 |
| 7398.004931 | 12.806 ± 0.04 | 7398.001829 | 12.082 ± 0.06 | 7398.007650 | 11.247 ± 0.06 |
| 7414.942199 | 13.232 ± 0.05 | 7414.939271 | 12.322 ± 0.05 | 7414.947569 | 11.626 ± 0.04 |
| 7415.920486 | 13.381 ± 0.05 | 7415.917326 | 12.580 ± 0.02 | 7415.923889 | 11.817 ± 0.04 |
| 7417.925231 | 13.424 ± 0.02 | 7417.922303 | 12.654 ± 0.03 | 7417.928264 | 11.817 ± 0.03 |
| 7418.876319 | 13.578 ± 0.03 | 7418.873403 | 12.664 ± 0.04 | 7418.879294 | 11.913 ± 0.03 |
| 7433.918194 | 12.006 ± 0.03 | 7433.915289 | 11.245 ± 0.05 | 7433.921042 | 10.495 ± 0.05 |
| 7435.834387 | 12.088 ± 0.04 | 7435.830475 | 11.228 ± 0.03 | 7435.837326 | 10.521 ± 0.03 |
| 7436.826690 | 12.143 ± 0.04 | 7436.823947 | 11.302 ± 0.04 | 7436.829780 | 10.569 ± 0.03 |
| 7441.708877 | 12.253 ± 0.04 | 7441.704965 | 11.447 ± 0.05 | 7441.712477 | 10.572 ± 0.04 |
| 7444.836910 | 12.197 ± 0.04 | 7444.833611 | 11.405 ± 0.04 | 7444.854340 | 10.583 ± 0.04 |
| 7447.826991 | 11.948 ± 0.06 | 7447.824155 | 10.949 ± 0.04 | 7447.829838 | 10.283 ± 0.06 |
| 7448.936030 | 11.835 ± 0.08 | 7448.933403 | 11.168 ± 0.03 | 7448.938426 | 10.923 ± 0.06 |
| 7466.799398 | 12.407 ± 0.05 | 7466.797257 | 11.529 ± 0.04 | 7466.801898 | 10.900 ± 0.07 |
| 7481.836609 | 12.555 ± 0.05 | 7481.832928 | 11.748 ± 0.03 | 7481.840324 | 10.839 ± 0.04 |
| 7493.745822 | 12.729 ± 0.04 | ... | ... | 7493.748507 | 11.177 ± 0.04 |
| 7495.712326 | 12.816 ± 0.06 | 7495.709433 | 11.860 ± 0.04 | 7495.715336 | 11.017 ± 0.05 |
| 7496.726366 | 12.628 ± 0.05 | 7496.723634 | 11.828 ± 0.04 | 7496.729167 | 11.151 ± 0.03 |
| 7497.674780 | 12.762 ± 0.05 | 7497.671574 | 11.979 ± 0.06 | 7497.678252 | 11.191 ± 0.05 |
| 7688.011887 | 11.771 ± 0.02 | 7688.009560 | 10.996 ± 0.02 | 7688.014572 | 10.175 ± 0.04 |
| 7689.016863 | 11.685 ± 0.03 | 7689.014410 | 11.186 ± 0.03 | 7689.019595 | 10.263 ± 0.04 |
| 7689.987280 | 11.989 ± 0.04 | 7689.984850 | 11.066 ± 0.03 | 7689.990081 | 10.413 ± 0.07 |

Table 1
(Continued)

| JD (2,450,000+) | <i>J</i> (mag ± error) | JD (2,450,000+) | <i>H</i> (mag ± error) | JD (2,450,000+) | <i>K_s</i> (mag ± error) |
|--------------------|---------------------------|--------------------|---------------------------|--------------------|---------------------------------------|
| 7706.036991 | 11.966 ± 0.05 | 7706.034711 | 11.218 ± 0.03 | 7706.039618 | 10.622 ± 0.05 |
| 7761.922882 | 12.244 ± 0.05 | 7761.919039 | 11.343 ± 0.05 | 7761.925336 | 10.651 ± 0.06 |
| 7764.949549 | 12.146 ± 0.04 | 7764.946343 | 11.407 ± 0.05 | 7764.952697 | 10.689 ± 0.04 |
| 7771.945058 | 12.453 ± 0.05 | 7771.942164 | 11.682 ± 0.05 | 7771.948032 | 10.891 ± 0.04 |
| 7787.826586 | 12.221 ± 0.03 | 7787.823808 | 11.349 ± 0.03 | 7787.830648 | 10.695 ± 0.09 |
| 7789.911285 | 11.965 ± 0.03 | 7789.908889 | 11.197 ± 0.03 | 7789.913426 | 10.505 ± 0.07 |
| 7805.881574 | 12.336 ± 0.04 | 7805.878796 | 11.465 ± 0.04 | 7805.884873 | 10.884 ± 0.04 |
| 7816.843542 | 12.338 ± 0.02 | 7816.835741 | 11.626 ± 0.03 | 7816.840972 | 10.796 ± 0.04 |
| 7819.820799 | 12.464 ± 0.04 | 7819.817894 | 11.674 ± 0.02 | 7819.823704 | 10.937 ± 0.04 |
| 7827.787164 | 12.296 ± 0.02 | 7827.785694 | 11.551 ± 0.05 | 7827.793519 | 10.779 ± 0.02 |
| 7867.683866 | 13.316 ± 0.05 | 7867.682940 | 12.380 ± 0.03 | 7867.684958 | 11.730 ± 0.04 |
| 7878.738183 | 12.709 ± 0.04 | 7878.735405 | 12.022 ± 0.04 | 7878.741481 | 11.277 ± 0.03 |
| 8118.848299 | 12.734 ± 0.06 | 8118.841991 | 11.671 ± 0.03 | 8118.855289 | 11.068 ± 0.05 |
| 8140.908125 | 12.959 ± 0.07 | 8140.904005 | 12.053 ± 0.03 | 8140.914340 | 11.298 ± 0.06 |
| 8146.955255 | 12.654 ± 0.04 | 8146.950729 | 11.783 ± 0.03 | 8146.959248 | 10.834 ± 0.07 |
| 8198.785648 | 13.090 ± 0.04 | 8198.780880 | 12.240 ± 0.04 | 8198.787963 | 11.518 ± 0.03 |
| 8204.733993 | 13.100 ± 0.04 | 8204.732500 | 12.131 ± 0.04 | 8204.735880 | 11.191 ± 0.07 |
| 8244.759329 | 13.005 ± 0.03 | 8244.751019 | 12.212 ± 0.03 | 8244.765243 | 11.396 ± 0.03 |
| 8257.641424 | 13.353 ± 0.08 | 8257.636748 | 12.251 ± 0.04 | ... | ... |
| 8448.052188 | 13.321 ± 0.05 | 8448.048657 | 12.540 ± 0.04 | 8448.056215 | 11.604 ± 0.05 |
| 8540.875486 | 13.557 ± 0.05 | 8540.868669 | 12.692 ± 0.02 | 8540.882789 | 12.064 ± 0.03 |
| 8571.836053 | 13.390 ± 0.06 | 8571.829630 | 12.660 ± 0.04 | 8571.839583 | 11.838 ± 0.04 |
| 8575.706343 | 13.236 ± 0.05 | 8575.703264 | 12.495 ± 0.02 | 8575.707627 | 11.771 ± 0.06 |
| 8582.743125 | 13.254 ± 0.03 | 8582.737755 | 12.477 ± 0.03 | 8582.754028 | 11.796 ± 0.02 |
| 8602.656944 | 13.592 ± 0.03 | 8602.655394 | 12.838 ± 0.02 | 8602.665301 | 11.981 ± 0.04 |
| 8603.718380 | 13.572 ± 0.02 | 8603.711111 | 12.830 ± 0.03 | 8603.718056 | 12.094 ± 0.03 |
| 8612.695833 | 13.550 ± 0.03 | 8612.696748 | 12.770 ± 0.04 | 8612.702616 | 11.952 ± 0.05 |
| 8793.024757 | 12.790 ± 0.03 | 8793.027627 | 11.913 ± 0.03 | 8793.030104 | 11.239 ± 0.04 |
| 8835.048819 | 13.499 ± 0.02 | 8835.042002 | 12.719 ± 0.03 | 8835.056366 | 11.842 ± 0.03 |
| 8836.952037 | 13.448 ± 0.04 | 8836.945127 | 12.592 ± 0.03 | ... | ... |
| 8856.916563 | 12.925 ± 0.03 | 8856.905081 | 12.153 ± 0.05 | 8856.921759 | 11.375 ± 0.05 |
| ... | ... | 8863.001574 | 12.645 ± 0.06 | ... | ... |
| 8866.942558 | 13.043 ± 0.04 | 8866.938056 | 12.352 ± 0.04 | 8866.947674 | 11.474 ± 0.03 |
| 8881.957072 | 13.056 ± 0.03 | 8881.953681 | 12.666 ± 0.06 | 8881.960440 | 11.831 ± 0.06 |
| 8882.899502 | 13.105 ± 0.03 | 8882.893669 | 12.328 ± 0.04 | 8882.905775 | 11.594 ± 0.06 |
| 8884.899606 | 13.115 ± 0.02 | 8884.895359 | 12.413 ± 0.03 | 8884.898171 | 11.639 ± 0.03 |
| 8886.837674 | 13.259 ± 0.03 | 8886.832407 | 12.412 ± 0.04 | 8886.840556 | 11.788 ± 0.04 |
| 8893.913889 | 13.380 ± 0.03 | 8893.908657 | 12.659 ± 0.04 | 8893.914271 | 11.838 ± 0.04 |
| 8913.878137 | 13.207 ± 0.03 | 8913.867593 | 12.350 ± 0.04 | 8913.881528 | 11.519 ± 0.05 |
| 8928.769537 | 12.766 ± 0.05 | 8928.766505 | 11.987 ± 0.03 | 8928.774757 | 11.230 ± 0.04 |
| 9221.020752 | 12.674 ± 0.05 | 9221.014132 | 11.715 ± 0.04 | 9221.028171 | 10.984 ± 0.03 |
| 9267.925313 | 12.981 ± 0.08 | 9267.917847 | 12.149 ± 0.05 | 9267.933484 | 11.296 ± 0.06 |
| 9307.813889 | 12.817 ± 0.04 | 9307.809769 | 11.979 ± 0.05 | 9307.826227 | 11.153 ± 0.05 |
| 9308.819769 | 12.572 ± 0.05 | 9308.813831 | 11.820 ± 0.04 | 9308.825694 | 11.114 ± 0.06 |
| 9326.738912 | 13.472 ± 0.08 | 9326.736539 | 12.440 ± 0.04 | 9326.742685 | 11.831 ± 0.04 |
| 9342.718310 | 13.610 ± 0.05 | 9342.714676 | 12.813 ± 0.05 | 9342.721910 | 12.098 ± 0.06 |
| 9356.686979 | 13.136 ± 0.04 | 9356.675532 | 12.226 ± 0.04 | 9356.694931 | 11.443 ± 0.04 |
| 9359.721157 | 12.961 ± 0.03 | 9359.715139 | 12.215 ± 0.03 | ... | ... |
| 9367.672188 | 13.483 ± 0.07 | 9367.669433 | 12.510 ± 0.04 | 9367.676481 | 11.521 ± 0.07 |
| 9369.638414 | 12.971 ± 0.02 | 9369.632141 | 12.184 ± 0.03 | 9369.639965 | 11.399 ± 0.03 |
| 9382.641609 | 13.608 ± 0.06 | 9382.637188 | 12.669 ± 0.07 | 9382.647118 | 11.861 ± 0.07 |
| 9532.018325 | 12.995 ± 0.07 | 9532.014527 | 12.050 ± 0.04 | 9532.022374 | 11.211 ± 0.04 |

clearly seen that we have observed the blazar right in between its historically brightest and faintest states.

Visually, it appears from Figure 1 that the *J*, *H*, and *K_s* NIR bands follow the same variability pattern. To further examine the variability relations between these NIR bands, we performed DCF analyses using the zDCF method between these bands as shown in Figure 2. Strong correlations with zero lag are found in the different combination of all three NIR bands. These correlations strongly indicate that the emissions in

the *J*, *H*, and *K_s* bands are cospatial and emitted from the same population of leptons.

3.2.2. Color Variability

For the total duration of our observations of OJ 287, NIR color variations with respect to time (color versus time) and with respect to *H*-band magnitude (color versus magnitude) are displayed in Figures 3 and 4, respectively. On visual

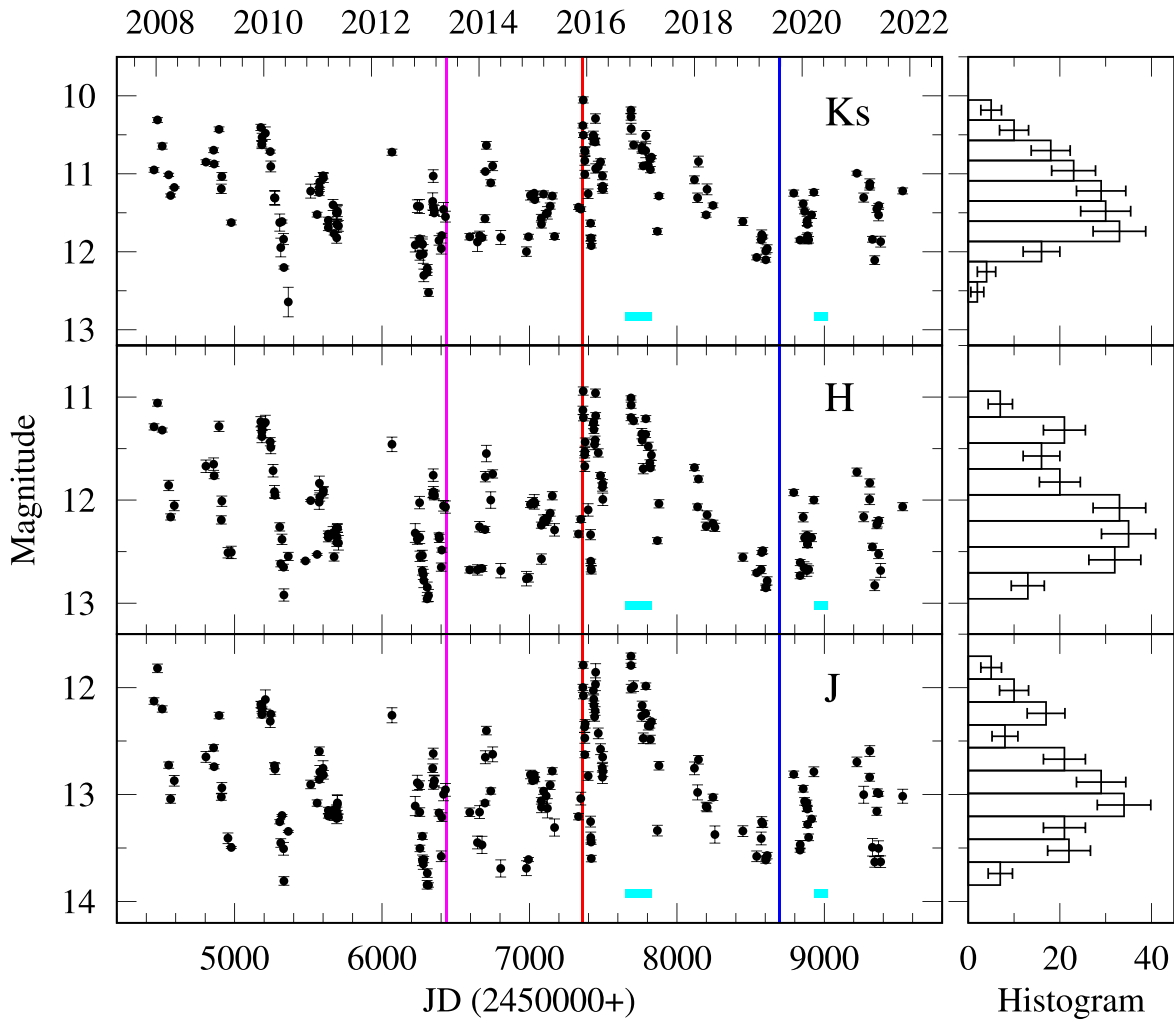


Figure 1. Multiband NIR variability LCs of the blazar OJ 287 during 2007 December–2021 November. From bottom to top, the left panels show J -, H -, and K_s -calibrated magnitudes, respectively. The right panels show how many measurements fall into each equal bin, the widths of which are assigned through the Knuth method (Knuth 2006) and differ slightly for each band. The magenta, red, and blue vertical lines, respectively, mark the first sighting of a rather sharp NIR–optical spectral break in end May 2013 and the flux peaks of the double-peaked outbursts of the ~ 12 yr QPO seen in end 2015 and mid-2019. The horizontal cyan lines mark the durations of the brightest X-ray activity phases as reported in the literature.

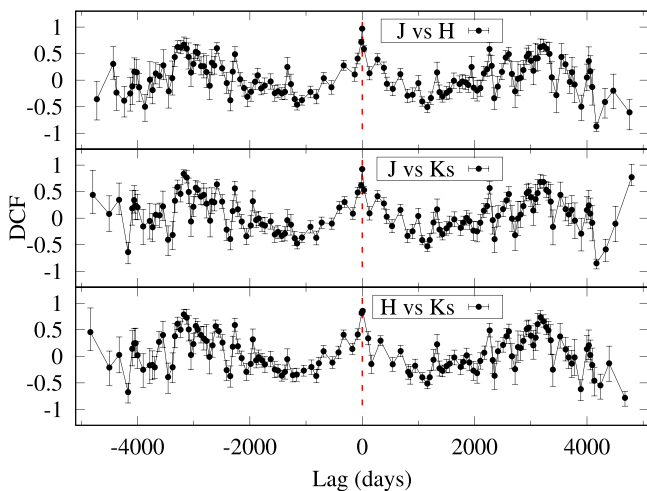


Figure 2. DCF plots using the zDCF method between NIR J , H , and K_s bands for the total duration of observations. The time-lag and DCF values are given on the x -axis and y -axis, respectively.

Table 2
Results of LTV Flux Variations

| Band | Duration | Variable | A (%) |
|-------|-----------------------|----------|---------|
| J | 2007-12-18–2021-11-13 | Var | 213.9 |
| H | 2007-12-18–2021-11-13 | Var | 201.4 |
| K_s | 2007-12-18–2021-11-13 | Var | 259.1 |

inspection both figures show weak evidence of color variations, but there are no consistent systematic trends in the color variations with respect to time or H -band magnitude. To further examine the color variation, we did straight-line fits to the color versus time, and color versus H -band magnitude, plots in Figures 3 and 4, respectively. The straight-line fit parameter values e.g., the slopes, m , the intercepts, c , the linear Pearson correlation coefficients, r , and the corresponding null hypothesis rejection probability, p , for color versus time and color versus H -band magnitude are given in Tables 3 and 4, respectively.

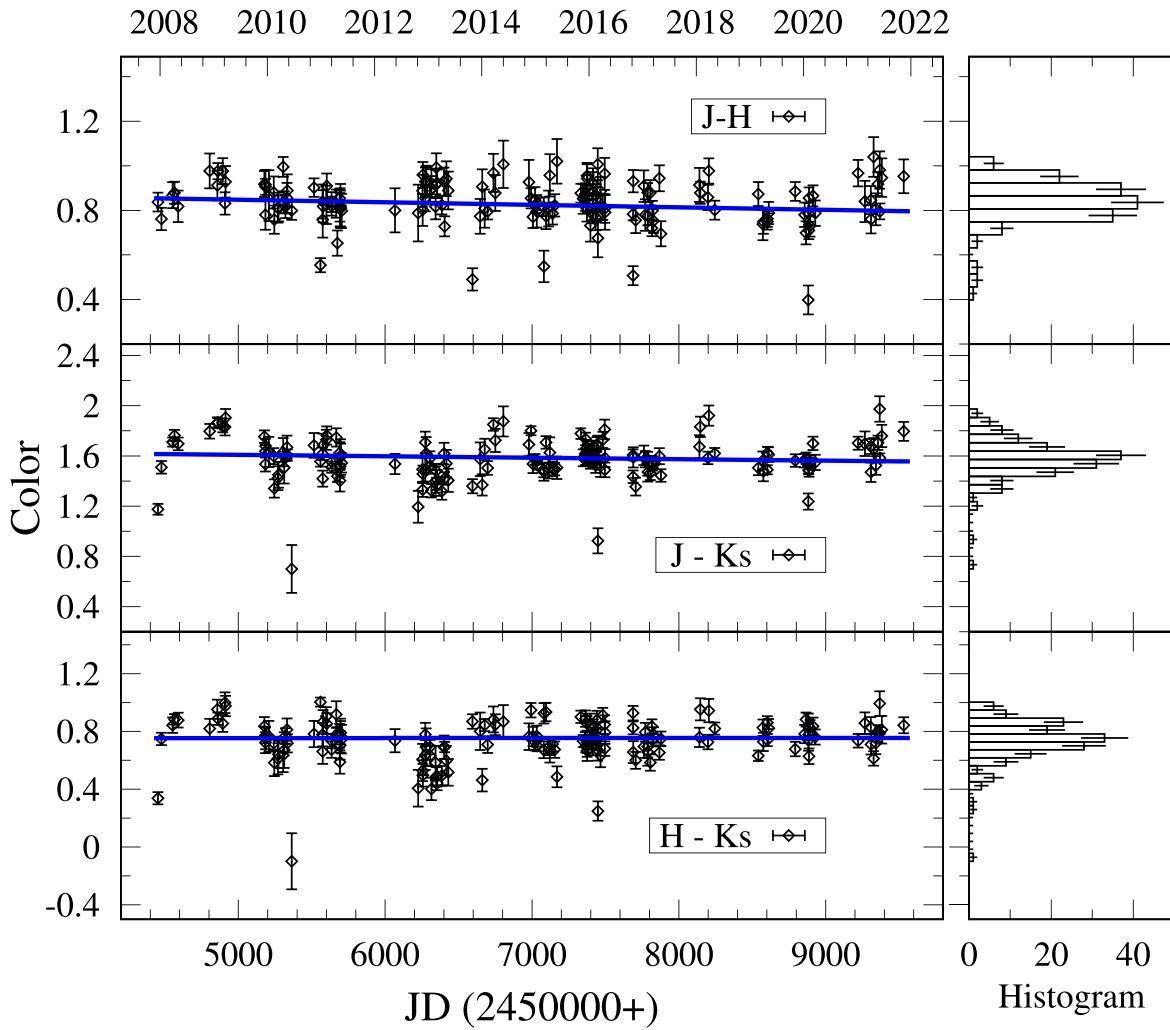


Figure 3. As in Figure 1 for the NIR color variability for the entire duration of these observations of OJ 287. The panels on the right show the spectral index histogram.

3.2.3. Spectral Index Variations and SEDs

In these magnitude measurements the color variations encode spectral information across the NIR. Making the assumption of a power-law spectrum across these bands we find

$$\alpha_{JKs} = \frac{(F_J/F_{Ks})}{(\nu_J/\nu_{Ks})}, \quad (4)$$

where F_J and F_{Ks} are fluxes calculated using the 2MASS zero values from Cohen et al. (2003) with respective central frequencies of these bands ν_J and ν_{Ks} . The reddening corrections for the J , H , and Ks bands are 0.02149, 0.01332, and 0.00874 mag, respectively (Cardelli et al. 1989, using $R_V = 3.1$ and $E(B - V) = 0.0241$).

Figure 5 shows these spectral changes with time as well as with source flux states in the J band. Neither of these show any systematic trend over the long term, as highlighted by the flat linear regression fits to them presented in Table 5. However, there are significant fluctuations around the mean, indicating spectral variations over short timescales as reflected in the histograms shown in the right panels of Figure 5. The histograms are skewed toward larger values of α_{Ks} indicating a tendency toward spectral steepening; however, there are a few instances showing spectral hardening.

The fluxes vary over almost an order of magnitude. The NIR SEDs, showing the diverse spectral facets exhibited by the source in between the minimum and maximum NIR flux states, are shown in Figure 6. The accompanying video presents a complete view of NIR SEDs with time. In general, the SEDs are flat or declining, with most being consistent with a power-law spectrum (within a 10% error). Occasionally, there are hints of smooth departures at the low-energy end as well of hardening.

3.2.4. Flaring and Outbursts

During the nearly 14 yr (2007 December–2021 November) of our intense multiband NIR observations of OJ 287 the source exhibited several well-defined large-amplitude flares seen in all these J , H , and Ks bands, plotted in Figure 1 from the bottom to top panels, respectively. We performed NIR interband cross correlation analysis using zDCF and plotted this in Figure 2. From Figure 2, we found that the J -, H -, and Ks -band fluxes are strongly correlated without any lag, so any observed flare in any of these J , H , and Ks bands are certainly observed quasi-simultaneously in the other two bands.

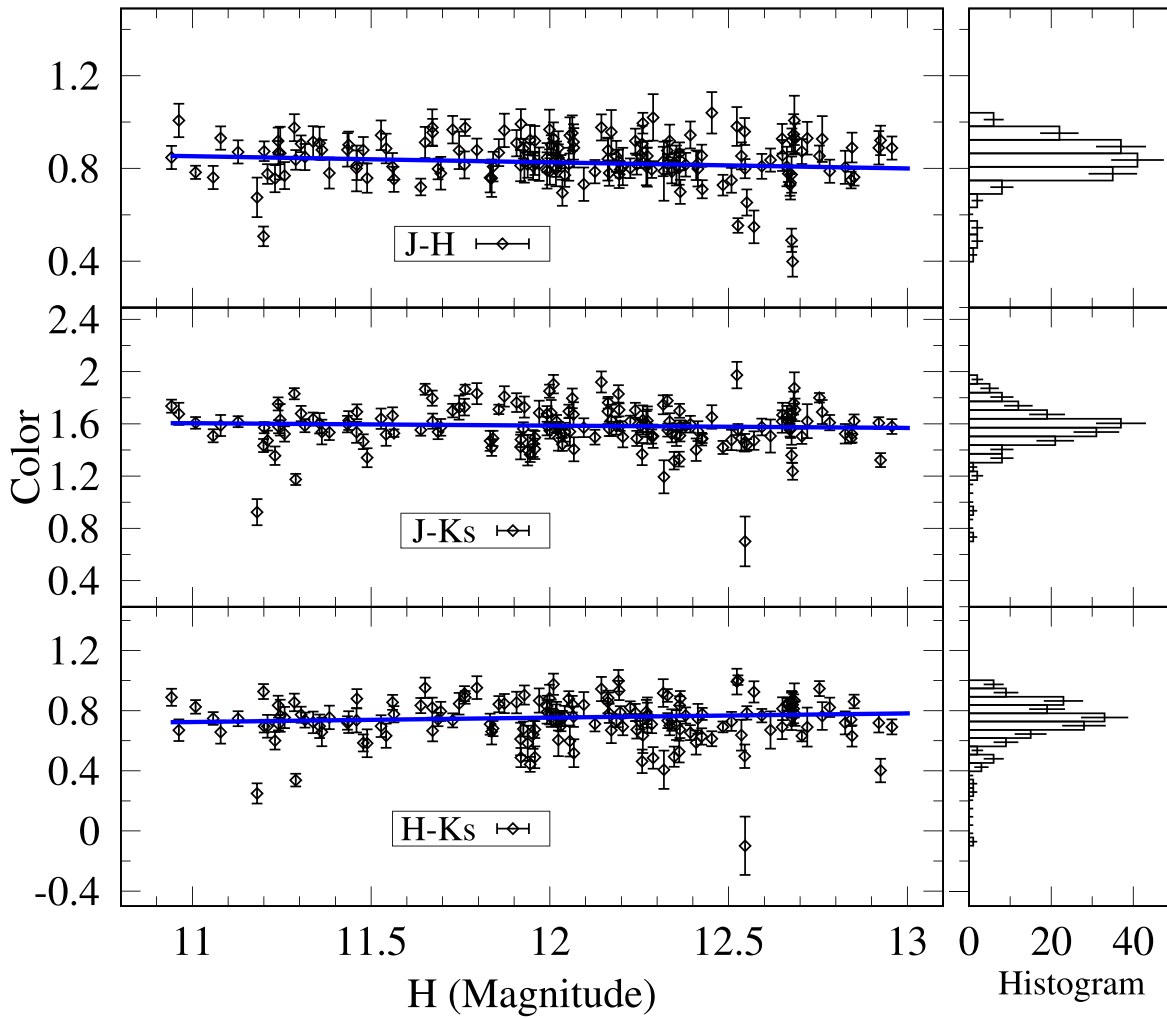


Figure 4. As in Figure 3 for NIR color–magnitude plots for OJ 287.

Table 3
Color Variation with Respect to Time on LTV

| Color Indices | $m_2 (\times 10^{-6})$ | c_2 | r_2 | p_2 |
|---------------|------------------------|-------------|--------|-------|
| $J - H$ | -11.3 ± 5.9 | 28 ± 14 | 0.017 | 0.06 |
| $J - K_s$ | -11.3 ± 8.0 | 29 ± 19 | 0.006 | 0.16 |
| $H - K_s$ | 0.31 ± 7.61 | 0 ± 18 | -0.006 | 0.97 |

Note. m_2 = slope and c_2 = intercept of color against H mag; r_2 = coefficient of determination (R^2); p_2 (0.05) = null hypothesis rejection probability.

4. Discussion

The current study presents the most up-to-date and extensive NIR spectral and temporal behavior of OJ 287 for the lengthy period of 2007 December–2021 November. Despite annual and inhomogeneous sampling-related gaps, the NIR fluxes are well sampled from high to low states, with denser sampling (~ 1 – 2 days interval) around and after the high states. This is true for almost every period of activity, as is clear from Figure 1.

The source has undergone strong and quite-frequent outbursts in NIR bands that are simultaneous within the observational cadence (Figure 2). The respective magnitude histograms are skewed, with more gradual falloffs on the brighter side but steeper declines on the fainter side. This

Table 4
Color Variation with Respect to H -band Magnitude on LTV

| Color Indices | m_2 | c_2 | r_2 | p_2 |
|---------------|--------------------|-----------------|--------|-------|
| $J - H$ | -0.026 ± 0.015 | 1.14 ± 0.18 | 0.013 | 0.08 |
| $J - K_s$ | -0.018 ± 0.022 | 1.80 ± 0.26 | -0.002 | 0.41 |
| $H - K_s$ | 0.028 ± 0.020 | 0.41 ± 0.24 | 0.007 | 0.16 |

Note. m_2 = slope and c_2 = intercept of color against H mag; r_2 = coefficient of determination (R^2); p_2 (0.05) = null hypothesis rejection probability.

skewness, however, is most likely from a sampling bias favoring brighter-state follow-up and could also have a minor effect from the change of base-level brightness, as discussed in the next paragraph. The time series reveal strong NIR flux variations with amplitudes almost similar to the optical bands of the same duration (Bonning et al. 2012; Sandrinelli et al. 2014; Gupta et al. 2017, 2019). There is almost an order of magnitude difference between the extremes (see Figure 6). Over long-term timescales, there is no systematic spectral evolution or trend either with time (Figure 3) or flux state of the source (Figure 4). However, during the bright phases, the flux changes are often associated with significant color variations over the short term, as highlighted by the fluctuations around

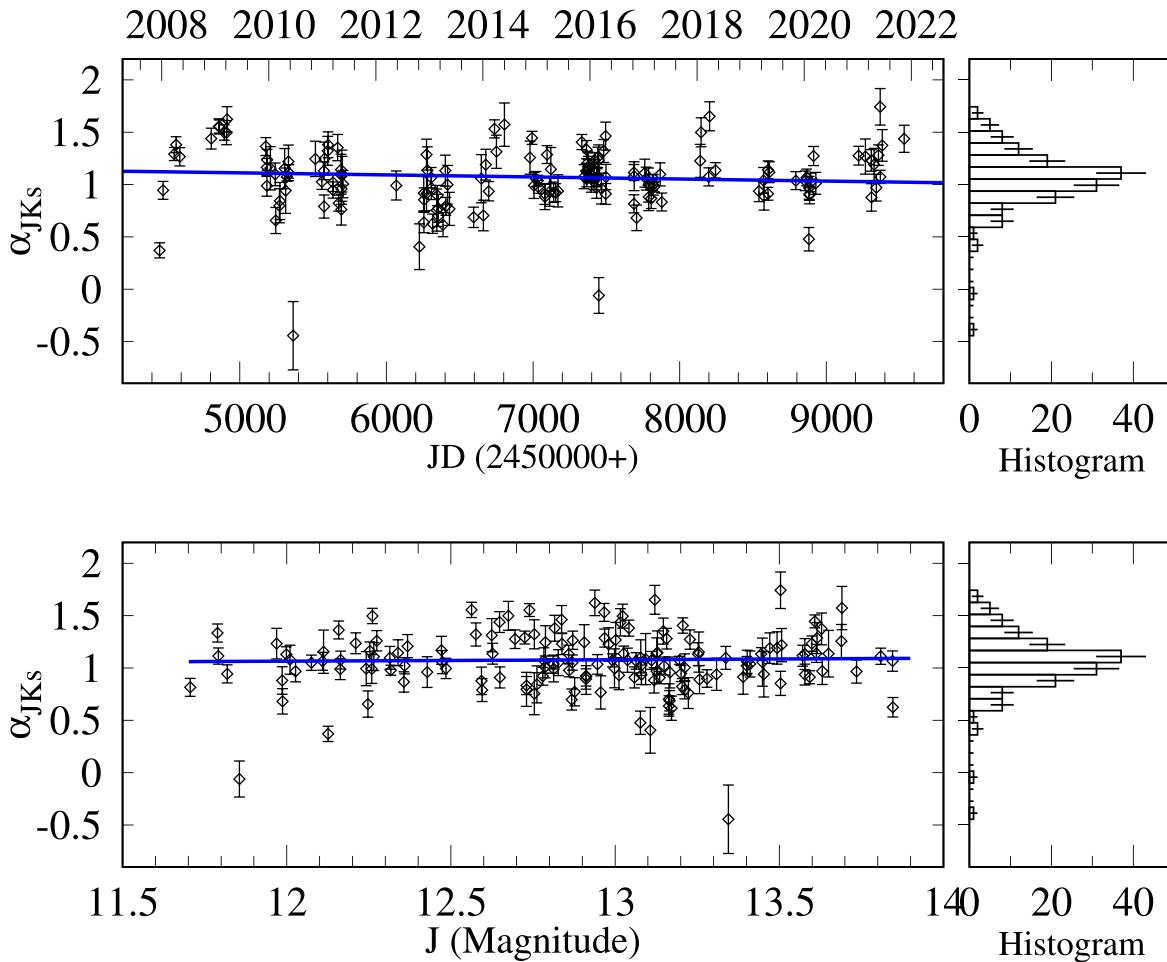


Figure 5. NIR spectral index variation with time and J -band magnitude covering the entire observation period of OJ 287. The panels on the right show the spectral index histogram.

Table 5

Spectral Index Variation with Respect to JD and J -band Magnitude for the Entire Period of the Observations of OJ 287

| Parameter | m_2 | c_2 | r_2 | p_2 |
|---------------------------------|---------------------------------|-----------------|--------|-------|
| α_{JKs} versus JD | $(-1.9 \pm 1.4) \times 10^{-5}$ | 48 ± 33 | 0.006 | 0.16 |
| α_{JKs} versus J (mag) | 0.014 ± 0.038 | 0.90 ± 0.49 | -0.006 | 0.72 |

Note. m_2 = slope and c_2 = intercept of α_{JKs} against JD or J ; r_2 = coefficient of determination (R^2); p_2 (0.05) = null hypothesis rejection probability.

the mean in the color (Figures 3 and 4) and spectral evolution plots (Figures 5 and 6). The color/spectral evolution with time and source brightness too are skewed, with a tendency for larger $J - H$ color/spectral variations indicating steepening of the spectrum with source brightness over short-term flaring episodes. Contrary to this general trend, a few instances show appreciable hardening (Figure 5).

The behaviors reported here are largely in line with those reported previously for OJ 287 at NIR bands (e.g., Zhang & Xie 1996; Fan et al. 1998; Bonning et al. 2012; Sandrinelli et al. 2014) and most of the seemingly contrary behavior can largely be attributed to sampling bias of the previous studies and the change in base-level brightness. For example, the typical brightness in the J , H , and Ks bands is 12.9, 12.0, and 11.3 mag with a typical standard variation of ~ 0.5 mag in each and a 2.0–2.5 mag

difference between the extremes. These brightness levels are in between the reported historical NIR brightness levels (1971 onwards) and so are the differences of the extremes (~ 3.5 mag; Fan et al. 1998). However, since both the NIR and optical emissions are synchrotron and lie on the extension of the same power-law spectral component (at and after the low-hump SED peak), the century-long optical LC can be used to examine any systematic/trends. This LC indicates a systematic decline of base-level brightness around 1 mag between 1971 and 2000 which reverses from 2000 onwards, with jet-related short-term and large-amplitude flares superposed on it (see Figure 1 of Dey et al. 2018). Thus, the variations and differences between the extremes are similar to those we see once the base brightness is taken into account. Similarly, the general tendency of larger $J - K/J - Ks$ color (indicating steepening of spectra) reported in earlier studies involving NIR and optical data (Zhang & Xie 1996, and references therein) is consistent with our results during flaring. The long-term systematic trend reported in Zhang & Xie (1996) is likely a sampling bias as is clear from the LC which shows a systematic decrease in flux before and after the most brightened event.

The current NIR observations are also the first NIR data taken during the brightest X-ray phases of this source that were seen in the years 2016–2017 and 2020 (Komossa et al. 2020)—a result of a new high-synchrotron-peaked BL Lac (HBL) type of broadband emission component (Kushwaha et al. 2018b,

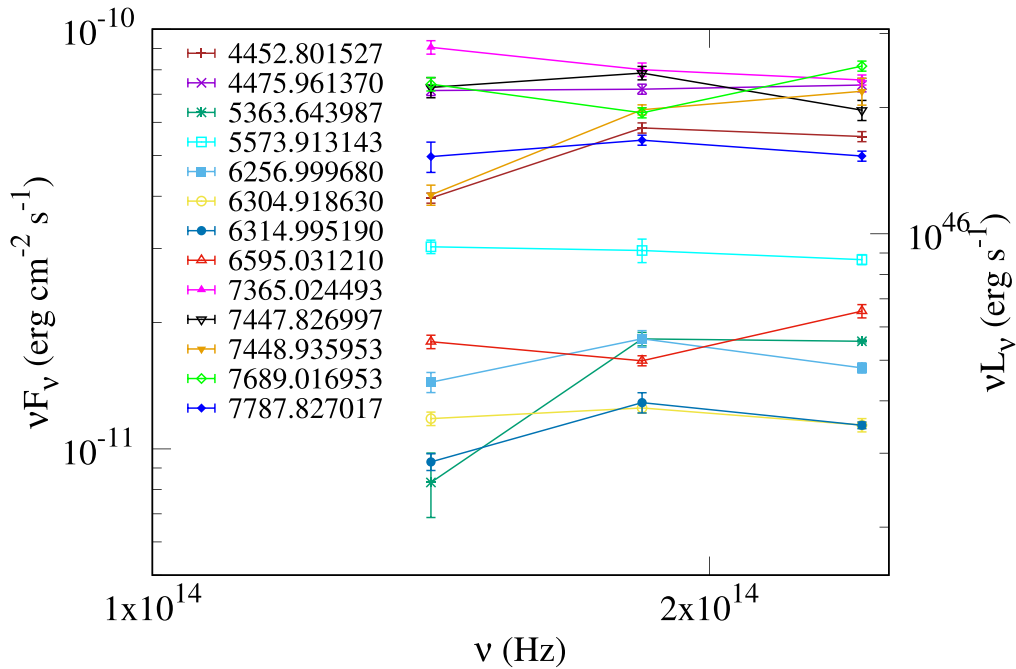


Figure 6. Plot showing a glimpse of diverse NIR spectral phases of OJ 287. The accompanying video shows the NIR SED evolution with time. The video duration is 17 s.

(An animation of this figure is available.)

2021; Singh et al. 2022). Both these bright X-ray phases came after the claimed double-peaked outbursts: the 2015 (Valtonen et al. 2016) and 2019 (Laine et al. 2020) flares of the ~ 12 yr optical QPOs. As the NIR variation amplitude is similar to that seen in the optical (Gupta et al. 2017, 2019) we can conclude that these overall variations are due to a jet emission component rather than the new, thermal-like, emission component seen during the 2013–2016 at the interface of the NIR–optical bands (Kushwaha et al. 2018a). This is also consistent with the brightest reported X-ray phases of the source being an HBL-like emission component.

Apart from these general trends, OJ 287 on short terms at different activity phases has shown very diverse and contrary behaviors. For example, none of the low-state SEDs presented here indicate any new emission component, but at most a spectral hardening; however, on a few occasions, NIR–optical data show otherwise (Sandrinelli et al. 2014). A hysteresis has also been reported involving redder-when-brighter and bluer-when-brighter trends as well as color changes at fixed magnitude (Bonning et al. 2012). The current observations also make it clear that the extreme and odd variability seen only in the K -band magnitude from the SMARTS¹³ database that persisted for almost an observing cycle (JD: $\sim 2,455,500$ – $2,455,710$), as reported in Kushwaha (2021), is most likely artificial. In short, although blazars are known for dynamic flux variability, they rarely show significant spectral departures in the broadband SEDs. OJ 287, on the other hand, is quite unique with spectral changes persisting for much longer time (e.g., Brien & VERITAS Collaboration 2017; Kushwaha et al. 2018a, 2018b, 2021; Prince et al. 2021; Singh et al. 2022) and thus, a potential source for fresh inputs not only on relativistic jets above what is generally known about blazars but also on aspects related to accretion as well (e.g., Kushwaha 2020, 2021).

5. Summary

We have presented the most up-to-date and extensive NIR observations of OJ 287 between 2007 and 2021. A summary of our results and inferences are as follows:

1. OJ 287 shows strong NIR variations with a brightness changes of $\gtrsim 2$ mag between the extremes. These variations are similar to those reported previously once the base-level brightness is taken out, as indicated by the optical LC exceeding a century in length.
2. The NIR variations are simultaneous within the limits of observational cadence.
3. There is no general tendency for color variations over this extended period either with the flux or with time. However, over short times (bright phases) the NIR spectrum steepens with brightness and vice versa. This tendency is similar to those reported in the literature in the optical and NIR bands.
4. A few of these observations show hardening of the NIR spectrum, possibly indicating a shift in the synchrotron SED peak, though they are not clearly significant.
5. The current NIR data includes the first data taken in these bands for bright X-ray phases. As those variabilities are similar to those in the optical they should arise from a broadband emission component.

The authors would like to dedicate this paper to the late Prof. S. S. Prasad who worked on exact solutions of Einstein’s equations. Prof. S. S. Prasad is acknowledged for inspiring his son A.C.G., the first author of this paper.

We thankfully acknowledge the anonymous reviewers for useful comments. P.K. acknowledges support from the Department of Science and Technology (DST), Government of India, through the DST-INSPIRE faculty grant (DST/INSPIRE/04/2020/002586). The INAOE, Mexico team






¹³ www.astro.yale.edu/smarts/glast/home.php

thanks CONACyT (Mexico) for the research grant CB-A1-S-25070 (Y.D.M.). H.G.X. is supported by the Ministry of Science and Technology of China (grant No. 2018YFA0404601) and the National Science Foundation of China (grants No. 11621303, 11835009, and 11973033). B.V. is funded by the Swedish Research Council (Vetenskapsrådet, grant No. 2017-06372). Z.Z.L. is thankful for support from the National Key R&D Programme of China (grant No. 2018YFA0404602) and the Talented Program from the Chinese Academy of Sciences (CAS).

Facilities: OAGH, CANICA.

Software: Astropy (Astropy Collaboration et al. 2013, 2018), statsmodel (Seabold & Perktold 2010), DAOPHOT (Stetson 1987), Gnuplot (v5.2; <http://www.gnuplot.info/>), IRAF (Tody 1986).

ORCID iDs

Alok C. Gupta  <https://orcid.org/0000-0002-9331-4388>
 Pankaj Kushwaha  <https://orcid.org/0000-0001-6890-2236>
 Haiguang Xu  <https://orcid.org/0000-0001-9405-0137>
 Paul J. Wiita  <https://orcid.org/0000-0002-1029-3746>
 Y. D. Mayya  <https://orcid.org/0000-0002-4677-0516>
 V. Chavushyan  <https://orcid.org/0000-0002-2558-0967>
 Zhongli Zhang  <https://orcid.org/0000-0002-8366-3373>

References

- Alexander, T. 1997, in *Astronomical Time Series*, ed. D. Maoz et al. (Dordrecht: Kluwer), 163
- Alexander, T. 2013, arXiv:1302.1508
- Astropy Collaboration, Price-Whelan, A. M., Sipőcz, B. M., et al. 2018, *AJ*, 156, 123
- Astropy Collaboration, Robitaille, T. P., Tollerud, E. J., et al. 2013, *A&A*, 558, A33
- Baker, J., Bellovary, J., Bender, P. L., et al. 2019a, arXiv:1907.06482
- Baker, J., Haiman, Z., Rossi, E. M., et al. 2019b, *BAAS*, 51, 123
- Bhatta, G., Zola, S., Stawarz, Ł., et al. 2016, *ApJ*, 832, 47
- Bonning, E., Urry, C. M., Bailyn, C., et al. 2012, *ApJ*, 756, 13
- Brien, S. O. & VERITAS Collaboration 2017, ICRC (Busan), 35, 650
- Britzen, S., Fendt, C., Witzel, G., et al. 2018, *MNRAS*, 478, 3199
- Burke-Spolaor, S., Taylor, S. R., Charisi, M., et al. 2019, *A&ARv*, 27, 5
- Butuzova, M. S., & Pushkarev, A. B. 2020, *Univ*, 6, 191
- Cardelli, J. A., Clayton, G. C., & Mathis, J. S. 1989, *ApJ*, 345, 245
- Carrasco, L., Dultzin-Hacyan, D., & Cruz-Gonzalez, I. 1985, *Natur*, 314, 146
- Carrasco, L., Hernández Utrera, O., Vázquez, S., et al. 2017, *RMxAA*, 53, 497
- Chen, J.-W., & Zhang, Y. 2018, *MNRAS*, 481, 2249
- Cohen, M., Wheaton, W. A., & Megeath, S. T. 2003, *AJ*, 126, 1090
- Dey, L., Valtonen, M. J., Gopakumar, A., et al. 2018, *ApJ*, 866, 11
- Epstein, E. E., Fogarty, W. G., Hackney, K. R., et al. 1972, *ApJL*, 178, L51
- Fan, J. H., Adam, G., Xie, G. Z., et al. 1998, *A&AS*, 133, 163
- Fossati, G., Maraschi, L., Celotti, A., et al. 1998, *MNRAS*, 299, 433
- Gear, W. K., Robson, E. I., & Brown, L. M. J. 1986, *Natur*, 324, 546
- Gupta, A. C., Agarwal, A., Mishra, A., et al. 2017, *MNRAS*, 465, 4423
- Gupta, A. C., Banerjee, D. P. K., Ashok, N. M., et al. 2004, *A&A*, 422, 505
- Gupta, A. C., Gaur, H., Wiita, P. J., et al. 2019, *AJ*, 157, 95
- Heidt, J., & Wagner, S. J. 1996, *A&A*, 305, 42
- Holmes, P. A., Brand, P. W. J. L., Impey, C. D., et al. 1984a, *MNRAS*, 210, 961
- Holmes, P. A., Brand, P. W. J. L., Impey, C. D., et al. 1984b, *MNRAS*, 211, 497
- Kidger, M. R., Gonzalez-Perez, J. N., de Diego, J. A., et al. 1995, *A&AS*, 113, 431
- Knuth, K. H. 2006, arXiv:physics/0605197
- Komossa, S., Grupe, D., Parker, M. L., et al. 2020, *MNRAS*, 498, L35
- Komossa, S., Grupe, D., Schartel, N., et al. 2017, in *IAU Symp. 324, New Frontiers in Black Hole Astrophysics* (Cambridge: Cambridge Univ. Press), 168
- Kushwaha, P. 2020, *Galax*, 8, 15
- Kushwaha, P. 2021, arXiv:2110.10851
- Kushwaha, P., Gupta, A. C., & Wiita, P. J., et al. 2018a, *MNRAS*, 473, 1145
- Kushwaha, P., Gupta, A. C., Wiita, P. J., et al. 2018b, *MNRAS*, 479, 1672
- Kushwaha, P., Pal, M., Kalita, N., et al. 2021, *ApJ*, 921, 18
- Kushwaha, P., Sarkar, A., Gupta, A. C., et al. 2020, *MNRAS*, 499, 653
- Laine, S., Dey, L., Valtonen, M., et al. 2020, *ApJL*, 894, L1
- Lehto, H. J., & Valtonen, M. J. 1996, *ApJ*, 460, 207
- Litchfield, S. J., Robson, E. I., & Stevens, J. A. 1994, *MNRAS*, 270, 341
- Marscher, A. P. 1983, *ApJ*, 264, 296
- Miller, H. R., Carini, M. T., & Goodrich, B. D. 1989, *Natur*, 337, 627
- Mücke, A., Protheroe, R. J., Engel, R., et al. 2003, *Aph*, 18, 593
- O'Brien, S. 2017, arXiv:1708.02160
- Pal, M., Kushwaha, P., Dewangan, G. C., et al. 2020, *ApJ*, 890, 47
- Prince, R., Agarwal, A., Gupta, N., et al. 2021, *A&A*, 654, A38
- Pursimo, T., Takalo, L. O., Sillanpää, A., et al. 2000, *A&AS*, 146, 141
- Romero, G. E., Boettcher, M., Markoff, S., et al. 2017, *SSRv*, 207, 5
- Sandrinelli, A., Covino, S., & Treves, A. 2014, *A&A*, 562, A79
- Seabold, S., & Perktold, J. 2010, *Proc. 9th Python in Science Conf.*, ed. S. van der Walt & J. Millman., 92
- Sillanpää, A., Haarala, S., Valtonen, M. J., et al. 1988, *ApJ*, 325, 628
- Sillanpää, A., Takalo, L. O., Pursimo, T., et al. 1996a, *A&A*, 305, L17
- Sillanpää, A., Takalo, L. O., Pursimo, T., et al. 1996b, *A&A*, 315, L13
- Singh, K. P., Kushwaha, P., Sinha, A., et al. 2022, *MNRAS*, 509, 2696
- Sitko, M. L., & Junkkarinen, V. T. 1985, *PASP*, 97, 1158
- Stetson, P. B. 1987, *PASP*, 99, 191
- Takalo, L. O., Kidger, M. R., de Diego, J. A., et al. 1992, *AJ*, 104, 40
- Tody, D. 1986, *Proc. SPIE*, 627, 733
- Urry, C. M., & Padovani, P. 1995, *PASP*, 107, 803
- Valtaoja, E., Lehto, H., Teerikorpi, P., et al. 1985, *Natur*, 314, 148
- Valtonen, M. J., Nilsson, K., Villforth, C., et al. 2009, *ApJ*, 698, 781
- Valtonen, M. J., Zola, S., Ciprini, S., et al. 2016, *ApJL*, 819, L37
- Visvanathan, N., & Elliot, J. L. 1973, *ApJ*, 179, 721
- Wagner, S. J., & Witzel, A. 1995, *ARA&A*, 33, 163
- Wolstencroft, R. D., Gilmore, G., & Williams, P. M. 1982, *MNRAS*, 201, 479
- Woo, J.-H., & Urry, C. M. 2002, *ApJ*, 579, 530
- Zhang, Y.-H., & Xie, G.-Z. 1996, *A&AS*, 119, 199